RSC Advances

ROYAL SOCIETY OF CHEMISTRY

www.rsc.org/advances

RSC Advances

ARTICLE

In situ dispersion of oil-based Ag nanocolloids by microdroplet coalescence and their applicaions in SERS detection

Received 00th January 20xx,
Accepted 00th January 20xx

DOI: 10.1039/x0xx00000x

www.rsc.org/

L. Du,[a] Y. J. Wang,[b] K. Wang,[b] C. Shen,*[c] and G. S. Luo*[b]

Monodispersity and size uniformity of the nanoparticles coated on film-like nanosensors are critical for the detection efficiency. However, there is limited controllability in the dispersion of these nanoparticles during their preparation and surface modification processes. Herein, we have developed a method for in situ dispersion of surface-modified Ag nanoparticles by controlling microdroplet coalescence, and fabricated surface-enhanced Raman scattering (SERS) films by spin-coating the nano-Ag suspensions. In the dispersion process, a two-plate type microchannel was employed to promote microdroplet coalescence. Under the experimentally optimized conditions, about 88% surface-modified Ag nanoparticles with an average size of 16−19 nm could be in situ dispersed. Upon the deposition of the resulting nanosuspensions on PDMS film surfaces, the films could be used to detect a target analyte, rhodamine 6G (R6G), at a detection limit of approximately 1.0×10^{-8} mol/L. The Ag-coated films were also confirmed to be stable and highly reusable.

1. Introduction

Nanosensors have emerged as a promising tool for a variety of applications such as monitoring physical and chemical phenomena, detecting biochemicals in cellular organelles, and measuring nanoparticles in industrial environments.[1–3] Specifically, film-like nanosensors have recently gained attention as they can rapidly detect hazard or contaminant for food industries, which have a great need for timely and efficient detection of food-borne pathogens by novel sensors and sensing systems enabled by molecular recognition methods or label-free transduction techniques.[4,5] Typical materials used for film-like nanosensors include polymers such as polydimethylsiloxane (PDMS), polymethylmethacrylate (PMMA), and polypropylene (PP) to serve as the support film, and nanoparticles such as gold, silver, and magnetic oxide nanoparticles to acquire the response signal.[6–10]

Through a spin- or dip-coating process, nanoparticles could be deposited onto the transparent film and then be coupled with spectrographic or chromatographic equipment for rapid detection. The film-like nanosensors require an effective deposition of highly monodispersed nanoparticles that permits accurate detection and resolution of changes in conductivity and absorption induced by analyte adsorption onto the nanoparticle surfaces.[11,12] The nanoparticles are usually produced and modified in the form of dry hydrophobic powder first, and then dispersed into organic phase. Subsequently, the support film is coated with the prepared nanosuspension and sent to drying or evaporation process to obtain the final products. In this case, the nanoparticles tend to agglomerate and sediment after being added into the organic liquid because of their poor compatibility. Research is therefore directed towards the one-step synthesis that consists of simultaneously generating and in situ dispersing the particles into organic phase.[13,14] In this method, processes of drying, storage, transportation, and dispersion of nanoparticles are avoided, so that the agglomeration of nanoparticles is reduced and the stability of nanosuspension can also be increased. For instance, Bakar *et al.*[15] developed a sensor system for the detection of pesticides by evaluating the effect of analytes on photoluminescence intensity of a film coated with ZnCdSe quantum dot, which were produced via an in situ dispersion process. Similarly, a homogenous GaP-coated film, unlike the case of the film surface being illuminated in a regular optoelectronic device, offered potential for trapping the incident photons through subwavelength diffractive effects between the nanowires.[16] Attempts have also been reported to deposit such coatings using SnO_2, Ag, Au, or Sn colloidal solutions via emulsion or microemulsion methods.[17–20] They confirmed that with the increase in monodispersity of nanoparticles on film surfaces, the resolution of hazards could be correspondingly increased by 50−300 % for surface-enhanced Raman scattering (commonly known as SERS) or fluorescence spectra.

Despite the intensification of rapid mixing by the microemulsion method, it is of common occurrence that the

[a] The State Key Laboratory of Chemical Resource Engineering, Beijing Key Laboratory of Membrane Science and Technology, Beijing University of Chemical Technology, Beijing 100029, China
[b] The State Key Laboratory of Chemical Engineering, Department of Chemical Engineering, Tsinghua University, Beijing 100084, China. E-mail: gsluo@tsinghua.edu.cn.
[c] Beijing Key Laboratory of Bioprocess, College of Life Science and Technology, Beijing University of Chemical Technology, Beijing 100029, China. E-mail: shenchun@mail.buct.edu.cn.

residual reactants, excess surfactant, and co-surfactant tend to be left in colloidal solutions due to the incomplete reaction or the stabilization effect of surfactants. The addition of co-surfactant, which is necessary for stabilizing microemulsions, is also detrimental to grafting biomacromolecules onto particle surfaces for specific demands.[21,22] On the other hand, for the emulsion systems, the problem stems from the difficulty of micrdoplet coalescence due to the stabilization effect by the surface-modified nanoparticles, accompanied by the formation of Pickering emulsions.[23] Therefore, the efficiency of interphase mass transfer of nanoparticles is significantly reduced, even with the employment of the reverse micelle method.[24,25]

In the past decade, several studies have focused on the coalescence behavior in microchannels, in which the microdroplets could deform significantly and collide frequently with each other by virtue of the confining boundaries.[26] Especially in recent years, initiation of microdroplet coalescence based on changing the interfacial tension gradient of microchannels has attracted considerable attention. On account of the high tension gradient due to the opposite wettabilities of microchannel walls (for example, a microchannel with stainless steel and PMMA plates).[27] In this case, slip flow can form at a unilateral side, leading to an alteration of the velocity profile of the fluid and microdroplet coalescence.[28] This novel strategy for in situ dispersion of modified nanoparticles would be an attractive alternative for preparation of the colloidal suspensions used for spin- or dip-coating. As such, we suggest developing the method of in situ dispersion of surface-modified nanoparticles by enhancing microdroplet coalescence.

In this study, we present an approach to prepare an Ag nanodispersion as the precursor colloidal solution based on in situ dispersion of surface-modified particles by microdroplet coalescence. A model system of SERS substrate, namely a PDMS film coated with Ag nanoparticles, was employed to investigate the effect of the dispersion method on the particle properties and the detection efficiency of the composite film. Accordingly, rhodamine 6G (R6G) was chosen as the target analyte. The influences of the particle size and dispersity were experimentally quantified. Finally, the detection efficiency of the Ag-based PDMS films was characterized by Raman spectroscopy and the influence of the particle property was experimentally quantified.

2. Experimental

2.1 Materials

Silver nitrate ($AgNO_3$, 99.8 %), ascorbic acid ($C_6H_8O_6$, 99.6 %), ethanol (99.8 %), acetone (99.6 %), *n*-hexane (99.5 %), and 3-amino-propyltriethoxysilane (96.0 %) were purchased from Beijing Chemical Works, Co. and used as received. The surface modifier, polyoxyethylene lauryl ether phosphate (98.5 %, AEO-9P), and the stabilizing agent, Daxad 19 (mol wt 8000), were purchased from Guangzhou Senda Co., as well as the analyte, rhodamine 6G (R6G, 99.0 %). Poly(dimethyl siloxane) (PDMS) films (with a thickness of 1 mm) were purchased from Shandong Xinyi Polymeric Material Co.

2.2 Apparatus

Fig. 1 illustrates the in situ dispersion route. A microchannel with two junctions was used to conduct the preparation (T-junction) and the in situ dispersion (sudden expansion) of Ag nanoparticles, respectively.

The bottom plate was fabricated from PDMS using soft lithography technique. At the T-junction, where the upper plate was also made of PDMS, the branch channels of equal size for dispersed phase flows were 200 μm × 200 μm (width × depth); while the main channel was 400 μm ×400 μm ×50 mm (width × depth × length). The in situ dispersion was directed by the sudden expansion, where the upper plate was made of glass. To seal the channel, the PDMS plate was first treated with a solution of sodium-naphthalene and then bonded with the upper glass plate. Prior to use, the sealed microchannel was washed with *n*-hexane to ensure that the plate surfaces had reverted to its initial wettability. The expanded section was 2 mm × 100 mm (width × length). A depth of 800 μm was chosen to provide a confinement space for the droplet coalescence. In addition, a circular hole (400 μm in diameter) and a square hole (4 mm × 4 mm in size) were milled for transport of recycle flows and observation of microdroplets with an embedded transparent glass plate.

2.3 Preparation of Ag nanoparticles

The surface-modified Ag nanoparticles were prepared using a precipitation method at room temperature. The mutually soluble aqueous solutions of $AgNO_3$ (0.1–0.8 mol/L) and $C_6H_8O_6$ (0.05–0.4 mol/L) serving as the dispersed phase were infused into the T-junction at the same flow rate of 50–200 μL/min, as shown in Fig. 1. Previously, AEO-9P was dissolved in the $C_6H_8O_6$ ethanol–water solution at a molar ratio of 2 × 10^{-3}:1 to Ag. Ag nanoparticles were prepared and simultaneously modified by the surfactant when the two dispersed fluids interacted with each other. The *n*-hexane as the continuous phase was infused at a flow rate of 100–2000 μL/min. In the T-junction, microdroplets of the aqueous

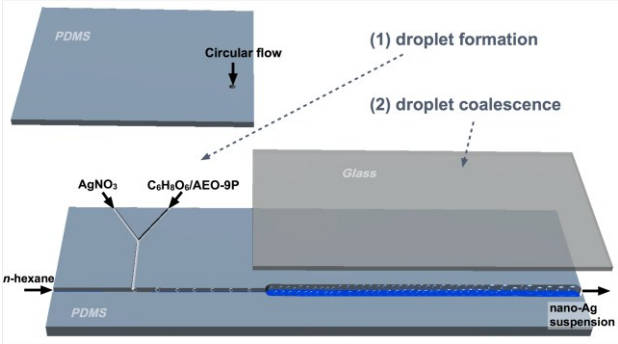

Fig. 1 Schematic diagram for the microchannel used in the preparation and dispersion of Ag nanocolloids.

solution were produced in the cross-flowing stream of *n*-hexane. The in situ dispersion was conducted immediately after the introduction of this fresh emulsion into the expanded section for droplet coalescence. By gathering the outflow using a volumetric glass vessel, we could obtain two phases: *n*-hexane (upper) and emulsion (bottom). The bottom layer was recycled back to the glass–PDMS channel for further demulsification. The circulation was not stopped until a homogeneous solution was finally obtained. Therefore, the coating suspensions with monodisperse Ag nanocolloids were prepared in the *n*-hexane.

For comparison, hydrophobic Ag nanoparticles have also been prepared without the coalescer, which is, in a subsequent dispersion process. In light of this preparation and dispersion procedure, only the two dispersed feeds mentioned above were infused and mixed to generate and modify the nanoparticles. The suspensions were collected at the outlet of the T-junction and agitated for 30 min. Then the precipitates were separated by centrifugation at 5000 rpm and then were washed several times with ethanol and deionized water. Finally, the modified Ag nanoparticles were added into *n*-hexane at the concentration according to the conditions of in situ dispersion.

2.4 Spin-coating of Ag nanocolloids and Arrangement of R6G specimen

The PDMS films were cut into approximately 5 cm × 5 cm pieces, cleaned with acetone, and then dried in air. Ag coatings were prepared via a spin-coating process on the films using 10 mL of the dispersion (form in situ and subsequent dispersion, respectively) at a speed of 1000 rpm for 30 s. After the spin-coating process, the films were placed in a drying oven maintained at 80 °C for 20 min in air to evaporate *n*-hexane, followed by UV exposure for 10 min to decompose surfactants on the particle-deposited surfaces of composite films. As a result, SERS films, on which Ag nanoparticles with varying amounts were loaded, were obtained as the final products.

Afterwards, we chose R6G as the analyte, which was commonly used to demonstrate the SERS effect of a substrate. About 1 mL of R6G in ethanol at different concentrations (from 0.5×10^{-8} to 6.5×10^{-6} mol/L) was dropped onto the Ag–PDMS film and was then dried in air for SERS detection.

2.5 Characterization methods

For visualization and droplet size estimation, micrographs of the microdroplets were taken using a JEOL-2010 microscope with a high-speed CCD camera (magnifications of 20–200 ×). A UV-Vis spectrophotometer (Agilent model 8453, Santa Clara) was also used to acquire the absorption spectra of Ag nanodispersions. X-ray diffraction (XRD) patterns of the Ag nanoparticles were measured from 2θ of 20°–80° (Rigaku Corporation D/max-RB). Transmission electron microscope (TEM) images of the particles were acquired on a JEOL 100CX operating at 100 keV.

Surface morphologies of the Ag-coated films were examined by atomic force microscopy (AFM; CypherTM, Asylum Research). Furthermore, to test the films for potential use as SERS substrates for detection of R6G, Raman spectra were measured using Raman spectrometer equipped with a diode laser (power 0.2 mW, wavelength 532 nm).[36–39] The specific surface area and the pore size distribution of the composite films were determined by a five-point Brunauer–Emmett–Teller (BET) method using a Quanttachrome autosorb-1 instrument.

3. Results and discussion

The droplet coalescence was utilized to enhance the dispersion of surface-modified Ag nanoparticles. To this end, operating conditions were examined to quantify their effects on both the coalescence and dispersion. The colloidal Ag dispersions and deposited films were characterized to evaluate the effect of dispersion processes on particle properties. Raman measurements were also conducted to verify the detection accuracy of the as-prepared SERS films.

3.1 Microdroplet coalescence and in situ dispersion

The efficiencies of droplet coalescence and dispersion of nanoparticles are defined to account for their relationship. The coalescence efficiency (E_C) is given by

$$E_C = \frac{V_{upper}}{V_{oil}} \times 100\% \quad (1)$$

where V_{upper} represents the volume of the oil phase (upper layer) phase and V_{oil} represents the total volume of *n*-hexane infused in the channel. The dispersion efficiency (E_T) of Ag particles can be calculated based on the solid content of the oil phase:

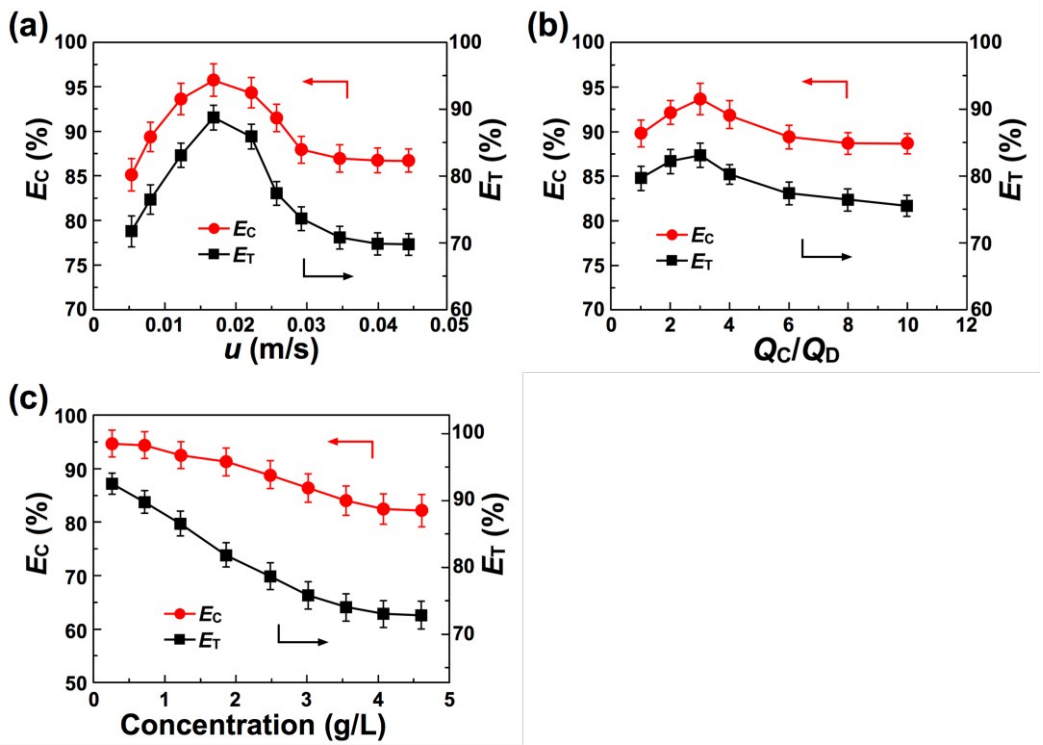

Fig. 2 Effects of flow velocity (a), phase ratio (b), and particle concentration (c) on microdroplet coalescence and particle dispersion efficiencies: (a) u varying, [$AgNO_3$] = 0.1 mol/L, [$C_6H_8O_6$] = 0.05 mol/L, Q_C/Q_D = 3; (b) Q_C/Q_D varying, [$AgNO_3$] = 0.1 mol/L, [$C_6H_8O_6$] = 0.05 mol/L, u = 0.017 ± 0.002 m/s; (c) particle concentration varying, u = 0.017 m/s, Q_C/Q_D = 3.

$$E_T = \frac{m_{upper}}{m_{particle}} \times 100\% \quad (2)$$

where m_{upper} denotes the mass of Ag nanoparticles in the oil phase and $m_{particle}$ denotes the total mass of the nanoparticles.

In Fig. 2a, the efficiencies of the coalescence and dispersion at varying flow velocities (u) are presented. The efficiencies follow quantitatively the same trend, indicating that the particle dispersion was enhanced by the droplet coalescence. E_C and E_T were found to increase from 0.005 to 0.017 m/s, but decrease to less than 82 % and 70 % after the velocity was increased to 0.044 m/s. This result can be explained if one considers not only the increase in the intensity of slip flow due to the high velocity, but also the decrease in residence time of the droplet flows. For the case of higher velocities, the residence time was greatly shortened. This limited the time of droplet collision, and as a result a droplet tended to brush past others, causing the dispersed phase to be of approximately the same volume fraction during circulation.

The results presented in Fig. 2b show the influence of the phase ratio (Q_C/Q_D, where Q_C represents the flow rate of the continuous phase and Q_D represents the flow rate of the dispersed phase) on the coalescence and dispersion efficiencies. Both E_C and E_T increased rapidly at low ratios (< 3) and decreased gradually at high ratios. Since the collision distance of the droplets was significantly reduced with the decrease of the phase ratio, coalescence could be correspondingly enhanced, causing an efficient mass transfer of hydrophobic nanoparticles into the oil phase. Meanwhile, the hydrophobic nanoparticles also tended to assemble at the superficial layer of *n*-hexane. As a result, maximum efficiencies were achieved at an oil–water phase ratio of approximately 3.

Particle concentration is also an important operating parameter for nanoparticle dispersion. A high concentration likely causes the assembly of nanoparticles at the interface, which is detrimental to the dispersion process. Fig. 2c shows the variations of E_C and E_T with respect to the particle concentration (the mass concentration of Ag nanoparticles in oil phase). Both E_C and E_T decreased with increasing concentration owing to the hindrance in mass transfer. Nevertheless, at a concentration of 4.7 g/L, E_C and E_T were still approximately 85 % and 80 % of their initial values, respectively. These results confirm the high efficiency of particle dispersion due to the microdroplet coalescence, even at the high concentrations when the hydrophobic nanoparticles could essentially stabilize water-in-oil emulsions.

Experiments of droplet size (d_p) distribution were conducted to find the variation of E_C and E_T during circulation. As can be seen from Fig. 3, most of the microdroplets had coalesced within 20 cycles. For the initial 8 cycles, a broader distribution was encountered predominantly and the droplets exhibited an average size of approximately 176 μm. Nevertheless, after 12 cycles, the distribution showed that smaller droplets had become dominant in the emulsion. Then a shift towards smaller droplet sizes was clearly evident, and after continuous circulation (about 20 cycles) the distribution was virtually dominated by a distinct fraction of microdroplets

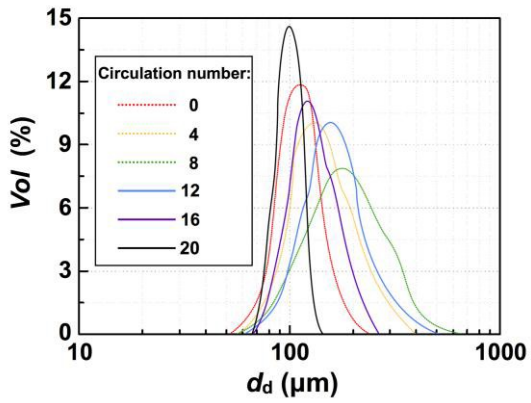

Fig. 3 Droplet size distributions of the collected solution at the outlet of the coalescer. Other conditions: [$AgNO_3$] = 0.1 mol/L, [$C_6H_8O_6$] = 0.05 mol/L, u = 0.017 m/s, Q_C/Q_D = 3.

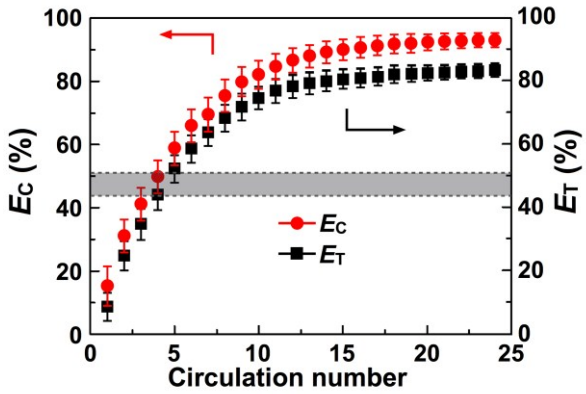

Fig. 4 The effects of circulation number of droplets passing through the coalescer on the dispersion efficiency. Other conditions: [$AgNO_3$] = 0.1 mol/L, [$C_6H_8O_6$] = 0.05 mol/L, u = 0.017 m/s, Q_C/Q_D = 3.

with a diameter of 97 μm. The dramatic change indicates that larger droplets had formed due to the occurrence of droplet coalescence at the beginning. Afterwards, the droplets were large enough to be separated in the vessel and only small droplets were recycled back into the coalescer, which was to be expected as continuous coalescence allowed the efficient phase separation to take place.

The effect of cycle number on E_C and E_T is shown in Fig. 4, where the grey region represents the value of E_T for the subsequent dispersion as a comparison. The variation of E_T is quite similar to that of E_C, which should be attributed to the timely removal of the hydrophobic nanoparticles at the interface. Within 20 cycles, E_T could reach a value of approximately 82 % while that of the subsequent dispersion was only about 43–51 %. The resistance to the particle dispersion was considered to be overcome due to the intensification by conducting microdroplet coalescence.

3.2 Characterization of Ag nanocolloids

The TEM images of the Ag nanocolloids obtained though different dispersion processes are shown in Fig. 5. In the case of the subsequent dispersion, the sample prepared at a higher concentration of 4.7 g/L (Fig. 5d) was composed of large particles of uneven size and with geometries on the order of approximately 30 nm, which was detrimental to SERS detection due to the large size.[29] Only at a lower concentration

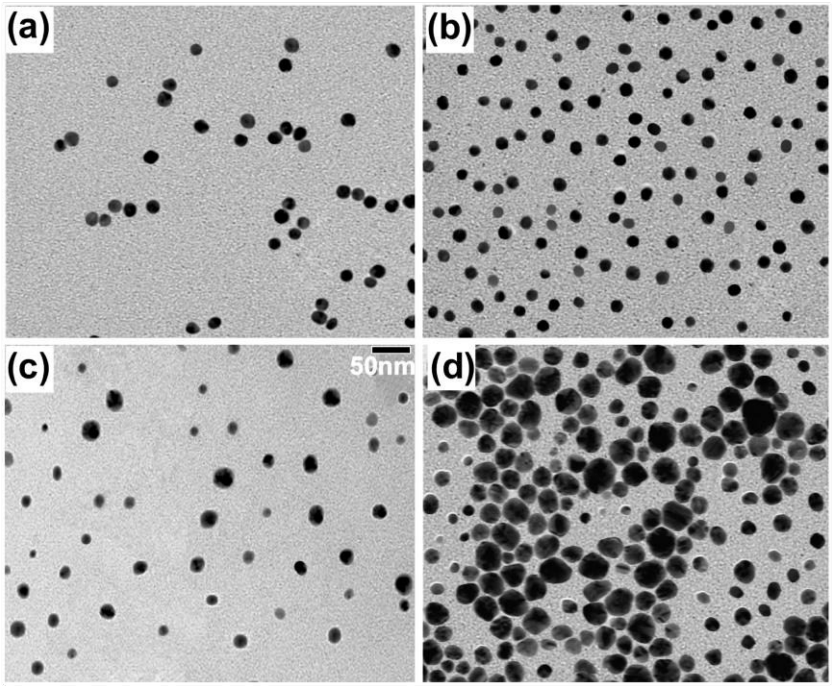

Fig. 5 TEM images of Ag nanoparticles obtained through different processes: (a) in situ dispersion, [Ag] = 0.7 g/L; (b) in situ dispersion, [Ag] = 4.7 g/L; (c) subsequent dispersion, [Ag] = 0.7 g/L; (d) subsequent dispersion, [Ag] = 4.7 g/L.

of 0.7 g/L, the Ag particles were much more uniform in size and their sizes could be reduced to the range of 10–20 nm. By contrast, upon in situ dispersion, monodispersed Ag nanoparticles with a uniform size could be controllably prepared (Figs. 5a and 5b). Even at the concentration of 4.7 g/L (Fig. 5b), the particles were apparently similar in size.

On the basis of measuring particle sizes (d_p, counting by ImageTool v3.0 with more than 200 particles for each sample) from the TEM images, their corresponding particle size distributions were obtained, as shown in Fig. 6. For the case of the in situ dispersion process, the samples exhibited a fairly uniform distribution of sizes between 10 and 20 nm, with an average diameter of about 16 nm (Fig. 6a) and 19 nm (Fig. 6b) for the low and high concentration conditions, respectively. It should be noted that the distribution (Fig. 6b) was barely altered by a 6-fold increase in the concentration, and was close to the result of the subsequent dispersion at the low concentration of 0.7 g/L (Fig. 6c). In comparison, the result of the subsequent dispersion at 4.7 g/L resulted in the appearance of a broader size distribution and a mean diameter of ca. 29 nm (Fig. 6d).

The XRD spectra of the Ag nanoparticles are shown in Fig. 7. The samples used for this characterization were sampled from the suspensions of 0.7 g/L and 4.7 g/L through different dispersion methods. The Ag particles are primarily of metallic silver phase, as evident from the comparison of diffraction peaks to the JCPDS database (No. 04-0783). All the characteristic peaks could be observed in the patterns at 2θ of 38.1°, 44.5°, 64.4°, and 77.4° corresponding to the diffractions of (111), (200), (220), and (311) planes. Pure phase could be achieved by both methods at different concentrations.

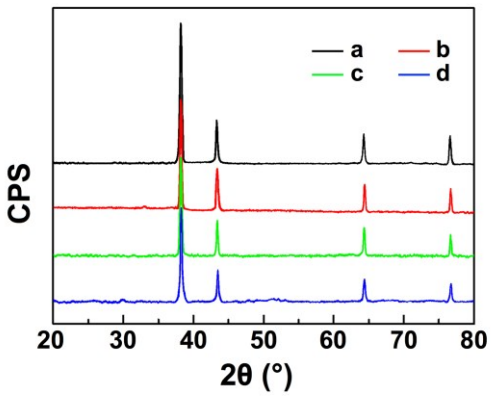

Fig. 7 XRD patterns of Ag nanoparticles. From top to bottom: (a) in situ dispersion, [Ag] = 0.7 g/L; (b) in situ dispersion, [Ag] = 4.7 g/L; (c) subsequent dispersion, [Ag] = 0.7 g/L; (d) subsequent dispersion, [Ag] = 4.7 g/L.

However, for the case of the in situ dispersion, a slight increase of the phase intensity was observed, indicating that rapid removal of surface-modified nanoparticles could prevent undesirable crystalline formation during the preparation.

UV-Vis absorption measurements were performed to investigate the properties of the dispersed nanoparticles in *n*-hexane, as shown in Fig. 8. All the samples were obtained from suspensions, which were prepared by the in situ and the subsequent dispersion methods. The absorption peaks at 400–420 nm correspond to spherical or spheroidal Ag nanoparticles with a characteristic size between 10 and 30

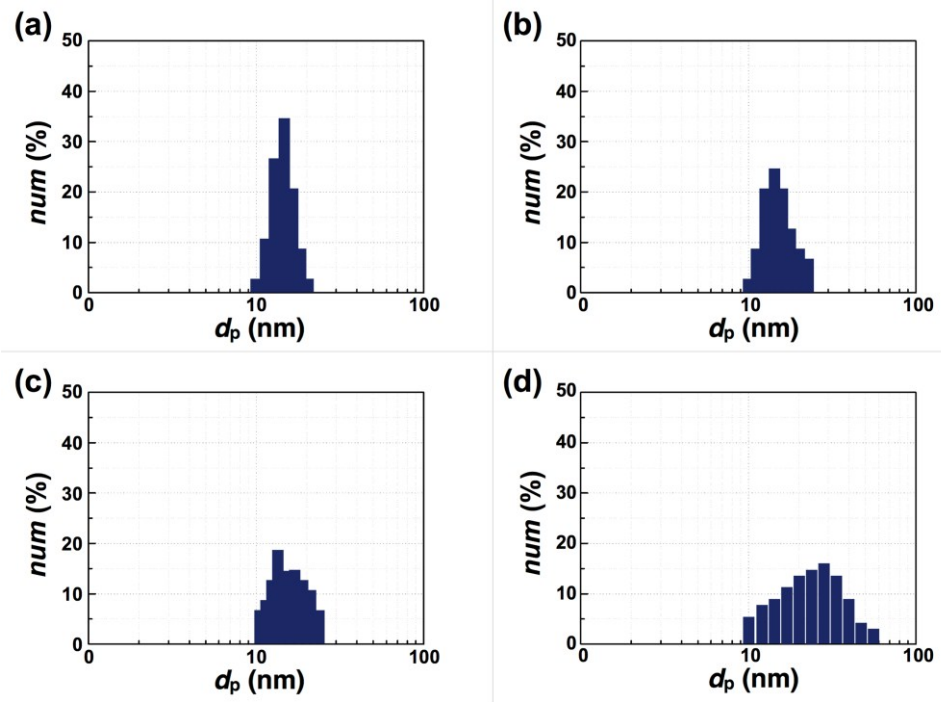

Fig. 6 Particle size distributions of Ag nanocolloids: (a) in situ dispersion, [Ag] = 0.7 g/L; (b) in situ dispersion, [Ag] = 4.7 g/L; (c) subsequent dispersion, [Ag] = 0.7 g/L; (d) subsequent dispersion, [Ag] = 4.7 g/L.

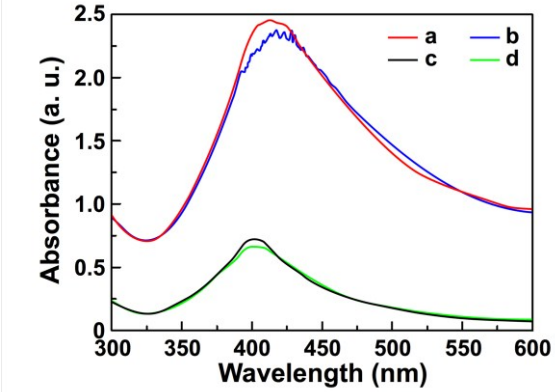

Fig. 8 Corresponding UV–vis spectra of Ag nanoparticles. From top to bottom: (a) in situ dispersion, [Ag] = 4.7 g/L; (b) subsequent dispersion, [Ag] = 4.7 g/L; (c) in situ dispersion, [Ag] = 0.7 g/L; (d) subsequent dispersion, [Ag] = 0.7 g/L.

nm.[30] At 0.7 g/L (curves a and c), the spectra are dominated by the Ag nanocolloids with an average size of about 15 nm. For the case of the higher concentration of 4.7 g/L, a ca. 10 nm bathochromic shift of the emission peak was observed for the in situ dispersed nanocolloids (curve b), while the bathochromic shift was as high as 30 nm for the subsequent dispersed nanocolloids (curve d), suggesting an increase of approximately 5 nm and 25 nm in colloidal size, respectively. This was mainly attributed to rapid removal of the interfacial nanoparticles by the in situ dispersion and thus the avoidance of particle growth and agglomeration. These results were corroborated by the results of the TEM images and the corresponding statistical results. Additionally, the widths of peaks, which were determined by particle size distribution, were also consistent with the results in Fig. 6.

3.3 Detection of R6G using Ag-based films

To estimate the SERS detection efficiency, the PDMS films were deposited with two concentrations of Ag nanosuspensions obtained from different dispersion processes. R6G was used as the model compound for SERS sensing. For each experiment, a 1 mL drop of the ethanol solution of R6G (2.2×10^{-8} mol/L) was placed on the PDMS film and spread to form a circular area. The morphologies of the Ag-coated films and the corresponding detection results are shown in Fig. 9. From Figs. 9b–e, one can see that the PDMS films, which were initially smooth and uniform (Fig. 9a), had been successfully deposited with Ag nanoparticles. In the case of in situ dispersion (Figs. 9b and 9c), the coated films appeared more uniform and there was hardly any area of delamination or degradation on them, which should be attributed to the avoidance of agglomeration by the rapid removal of the hydrophobic nanoparticles. The Ag-coated film with fewer particles had a slight change in surface roughness and coating layer microstructure (Fig. 9d) as compared with the in situ dispersion sample at the same concentration (Fig. 9b). However, with respect to the film coated by more subsequent dispersed particles, its cross-sectional results showed that the particles adsorbed on the surface featured a step height between 4 and 100 nm (Fig. 9e), which was 50 % larger than all the others, indicating that there existed agglomerates in the Ag layer. The Raman spectra revealed the general trend for an increase of SERS detection efficiency with an increase in particle monodispersity and size uniformity. As shown in Figs. 9b and 9c, well-resolved signatures of R6G at 5.0×10^{-7} mol/L could be readily observed, while the same experiment for the film coated with fewer subsequent dispersed particles (Fig. 9d) only yielded weak signals like that of the background (Fig. 9a). Apparently, with the effective deposition of monodispersed and uniformly distributed Ag nanoparticles, the Raman detection accuracy for R6G was twice as high as that of the sample with more agglomerates. As a matter of fact, the

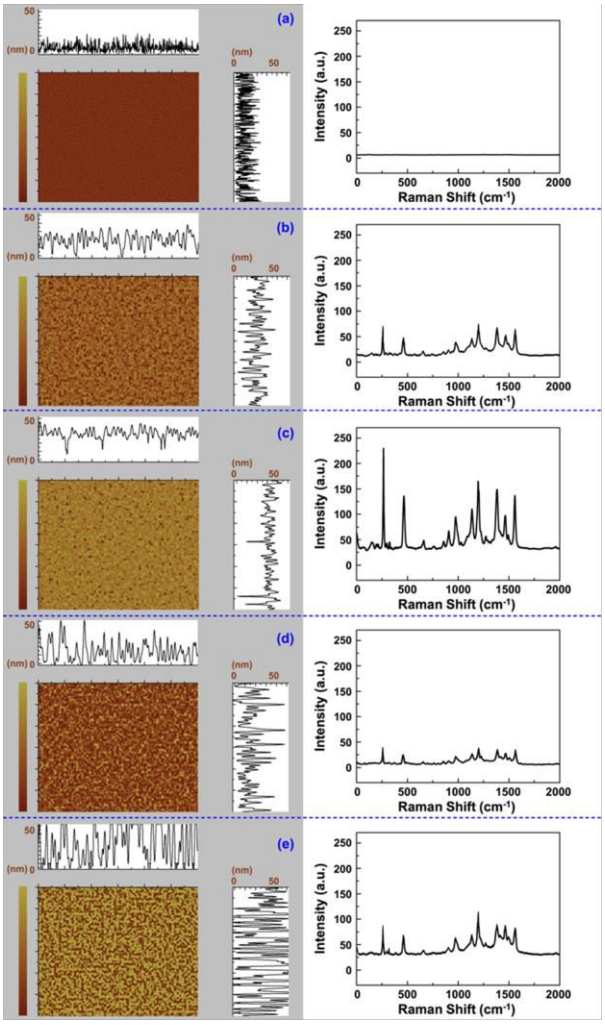

Fig. 9 AFM images of the PDMS films and corresponding SERS responses: (a) the initial PDMS film; (b) the PDMS film coated with the nano-Ag suspension of 0.7 g/L obtained by in situ dispersion; (c) the PDMS film coated with the nano-Ag suspension of 4.7 g/L obtained by in situ dispersion; (d) the PDMS film coated with the nano-Ag suspension of 0.7 g/L obtained by subsequent dispersion; (e) the PDMS film coated with the nano-Ag suspension of 4.7 g/L obtained by subsequent dispersion.

enhancement was caused by the increase in the contact area of nanoparticles and analytes (along with less agglomerates),[34,35] which should be attributed to the in situ dispersion of Ag nanoparticles. The values of specific surface area are shown in Fig. S1

Fig. 10 shows the relationship between the SERS intensity (at 1582 cm^{-1}, using the films with 4.7 g/L nanoparticles) and the concentration of R6G in ethanol, by which the detection limit could be calculated according to the minimum effective value of approximately 50 a.u. for the Raman intensity.[31] As can be seen, the intensity increases linearly as a function of the exponent of the R6G concentration. On the basis of the result of the sample obtained by in situ dispersion, a detection limit of approximately 1.0 × 10^{-8} mol/L (the corresponding Raman spectrum is shown in Fig. S2) could be achieved. For comparison, the Raman intensity of the sample obtained by subsequent dispersion increased gradually with increasing concentration. In this case, the film could detect the R6G at a minimum concentration of 2.0 × 10^{-8} mol/L. The SERS results (all the Raman spectra are shown in Fig. S4) confirmed the importance of particle monodispersity and distribution uniformity for detection efficiency. Compared with other studies, the SERS film prepared with the in situ dispersed Ag nanoparticles are capable of detecting R6G at a low detection limit, which is, approximately 1.0 × 10^{-8} mol/L compared to 1.0 × 10^{-8} to 1.0 × 10^{-7} mol/L with 30–80% less nanoparticles (per unit surface area) on the film.[7,31,32]The in situ dispersion method might offer some advantages such as lower amounts of noble metal and analyte, and higher sensitivity for their potential applications in rapid detection.

Furthermore, the Ag-coated SERS films were assumed to be stable against solvent washing and readily regenerated for repeated detection. As shown in Fig. 11, for the film coated with the in situ dispersed nanoparticles, the SERS response (obtained by tracing the peak intensity at 1582 cm^{-1}) to the 5.0 × 10^{-7} mol/L R6G solution remained unchanged after 15 cycles of ethanol rinsing. By contrast, for the film coated with subsequent dispersed particles, it was observed that the signal intensity decreased significantly with the circulation number. The signal attenuation was attributed to the loss of Ag nanoparticles from the film surface (the corresponding AFM images are shown in Fig. S3), because agglomerates had smaller contact area to the film and the attractive force was relatively weak in comparison to that of the in situ dispersed particles.[33]

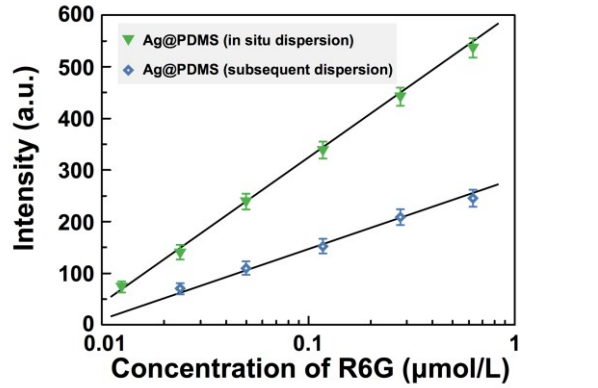

Fig. 10 Plot of the intensity of the 1582 cm^{-1} peak of R6G at varying concentrations using different SERS films.

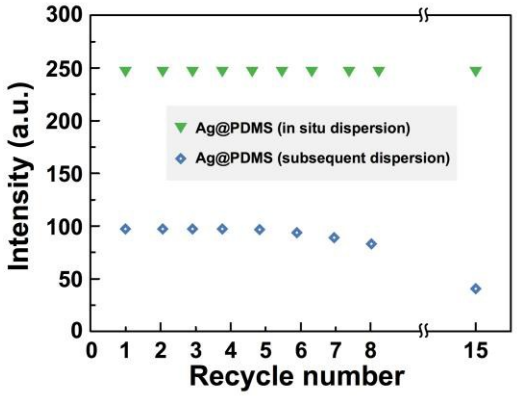

Fig. 11 SERS responses (traced by the peak signal at 1582 cm^{-1}) of different SERS films at the R6G solution of 5.0 ×10^{-7} mol/L during repeated cycles.

To sum up, the enhancement of detection efficiency of Ag-coated SERS films prepared by coating with the in situ dispersed particles was preliminarily confirmed. However, preparation of nano-Ag suspensions still requires further research because the concentration need considerably increasing, especially for their use in nanofluids and composite materials.

Conclusions

In this study, we have developed a strategy to in situ disperse surface-modified Ag nanoparticles into organic carriers and fabricate SERS films by dip-coating with the nanocolloidal suspensions. The in situ dispersion of nanoparticles was enhanced by initiating controllable microdroplet coalescence, which was successfully performed using the plate-type microchannel. By virtue of the simultaneous dispersion, the precursor nanosuspensions with monodispersed and uniformly distributed Ag nanoparticles could be controllably prepared. The experiments confirmed that, for the case of in situ dispersion under optimal conditions, about 88 % of the surface-modified Ag nanoparticles with an average size of 16–19 nm could be in situ dispersed and they could be readily deposited on the surfaces of PDMS films by spin-coating. The efficiency of the Ag-coated films for SERS detection of R6G as the analyte was evaluated, confirming that the films had a detection limit of approximately 1.0 × 10^{-8} mol/L. The films were also preliminarily confirmed to be stable against normal washing and highly reusable.

Although further optimization is still needed, the controllable dispersion of nanoparticles into precursor solutions by droplet coalescence might provide possibilities for continuous and quantitative preparation of nonaqueous

nanocolloids. Future studies should be focused on increasing the concentration of nanodispersions and the corresponding mechanism of the particle dispersion process.

Acknowledgements

We gratefully acknowledge the support of the National Basic Research Foundation of China (Grant No. 2013CB733600), the National Natural Science Foundation of China (91334201, 21036002, 21276140, 21506004), and the Fundamental Research Funds for the Central Universities of China (ZY1630).

Notation

[M] = molar concentration, M corresponds to the specific material
d_d = droplet size (μm)
d_p = nanoparticle size (nm)
E_C = efficiency of droplet coalescence (%)
E_T = efficiency of nanoparticle dispersion (%)
m = mass of Ag nanoparticles (g)
Q_C = flow rate of the continuous phase (mL/min)
Q_D = flow rate of the dispersed phase (mL/min)
u = average flow velocity (m/s)
V = volume fraction (%)

References

1 C. Y. Zhang, H. C. Yeh, M. T. Kuroki and T. H. Wang, *Nat. Mater.*, 2005, **4**, 826–831.
2 L. Chen, N. Qi, X. Wang, L. Chen, H. You and J. Li, *RSC Adv.*, 2014, **4**, 15055–15060.
3 M. Li, Q. Wang, X. Shi, L. A. Hornak and N. Wu, *Anal. Chem.*, 2011, **83**, 7061–7065.
4 Q. Gao, D. Luo, M. Bai, Z.-W. Chen and Y.-Q. Feng, *J. Agric. Food. Chem.*, 2011, **59**, 8543–8549.
5 L. Gao, X. Li, C. Li and Y. Yan, *RSC Adv.*, 2015, **5**, 96158–96164.
6 P. Quaresma, I. Osorio, G. Doria, P. A. Carvalho, A. Pereira, J. Langer, J. P. Araujo, I. Pastoriza-Santos, L. M. Liz-Marzan, R. Franco, P. V. Baptista and E. Pereira, *RSC Adv.*, 2014, **4**, 3659–3667.
7 S. Liu, C. Jiang, B. Yang, Z. Zhang and M. Han, *RSC Adv.*, 2014, **4**, 42358–42363.
8 H. G. Yoo, M. Byun, C. K. Jeong and K. J. Lee, *Adv. Mater.*, 2015, **27**, 3982–3998.
9 C. Geddes and K. Aslan, *J. Fluoresc.*, 2005, **15**, 99–104.
10 A. Lamberti, A. Virga, A. Angelini, A. Ricci, E. Descrovi, M. Cocuzza and F. Giorgis, *RSC Adv.*, 2015, **5**, 4404–4410.
11 Z. Wang, G. Meng, Z. Huang, Z. Li and Q. Zhou, *Nanoscale*, 2014, **6**, 15280–15285.
12 C. Liu, X. Zhang, L. Li, J. Cui, Y. Shi, L. Wang and J. Zhan, *Analyst*, 2015, **140**, 4668–4675.
13 L. Chen, L. Luo, Z. Chen, M. Zhang, J. A. Zapien, C. S. Lee and S. T. Lee, *J. Phys. Chem. C*, 2009, **114**, 93–100.
14 B. Peng, G. Li, D. Li, S. Dodson, Q. Zhang, J. Zhang, Y. Lee, H. Demir, X. Ling and Q. Xiong, *ACS Nano*, 2013, **7**, 5993–6000.
15 N. Bakar, M. Salleh, A. Umar and M. Yahaya, *Adv. Nat. Sci.*, 2011, **2**, 025011.
16 O. L. Muskens, S. L. Diedenhofen, B. C. Kaas, R. E. Algra, E. P. A. M. Bakkers, J. G. Rivas and A. Lagendijk, *Nano Lett.*, 2009, **9**, 930–934.
17 S. Anantharaj, U. Nithiyanantham, S. R. Ede and S. Kundu, *Ind. Eng. Chem. Res.*, 2014, **53**, 19228–19238.
18 A. Solieman, A. H. Moharram and M. A. Aegerter, *Appl. Surf. Sci.*, 2010, **256**, 1925–1929.
19 N. Zhang, X. Yu, J. Hu, F. Xue and E. Ding, *RSC Adv.*, 2013, **3**, 13740–13747.
20 H. Dridi, A. Moadhen and L. Haji, *J. Porous Mater.*, 2015, **22**, 239–245.
21 A. Rezvanpour and C.-H. Wang, *Chem. Eng. J.*, 2014, **239**, 8–18.
22 A. Jaroenworaluck, N. Pijarn, N. Kosachan and R. Stevens, *Chem. Eng. J.*, 2012, **181**, 45–55.
23 J.-W. Kim, A. Fernandez-Nieves, N. Dan, A. S. Utada, M. Marquez and D. A. Weitz, *Nano Lett.*, 2007, **7**, 2876–2880.
24 H. Yan, W. Pan, D. An-Ping, Y. Jing, H. Ying-Ping and Y. Yong, *J. Inorg. Mater.*, 2010, **25**, 1221–1226.
25 C. Singh, S. Bansal and S. Singhal, *Physica. B*, 2014, **444**, 70–76.
26 C. R. Vitasari, M. Gramblicka, K. Gibcus, T. J. Visser, R. Geertman and B. Schuur, *Sep. Purif. Technol.*, 2015, **155**, 58–65.
27 Y. Okubo, M. Toma, H. Ueda, T. Maki and K. Mae, *Chem. Eng. J.*, 2004, **101**, 39–48.
28 X. Chen, H. Lu, W. Jiang, L. Y. Chu and B. Liang, *Ind. Eng. Chem. Res.*, 2010, **49**, 9279–9288.
29 D. Ormerod, B. Bongers, W. Porto-Carrero, S. Giegas, G. Vijt, N. Lefevre, D. Lauwers, W. Brusten and A. Buekenhoudt, *RSC Adv.*, 2013, **3**, 21501–21510.
30 A. D. Ormonde, E. C. M. Hicks, J. Castillo and R. P. Van Duyne, *Langmuir*, 2004, **20**, 6927–6931.
31 E. Fazio, F. Neri, A. Valenti, P. M. Ossi, S. Trusso and R. C. Ponterio, *Appl. Surf. Sci.*, 2013, **278**, 259–264.
32 Y. Lin, C. E. Bunker, K. A. S. Fernando and J. W. Connell, *ACS Appl. Mater. Interfaces*, 2012, **4**, 1110–1117.
33 J. Parisi, L. Su and Y. Lei, *Lab. Chip.*, 2013, **13**, 1501–1508.
34 E.-C. Lin, J. Fang, S.-C. Park, F. W. Johnson and H. O. Jacobs, *Nat. Commun.*, 2013, **4**, 1636.
35 Y. L. Hu, J. Liao, D. M. Wang and G. K. Li, *Anal. Chem.*, 2014, **86**, 3955–3963.
36 H. Zhou, D. Yang, N. P. Ivleva, N. E. Mircescu, R. Niessner and C. Haisch, *Anal. Chem.*, 2014, **86**, 1525–1533.
37 H. A. Kashmery, D. G. Thompson, R. Dondi, S. Mabbott, D. Graham, A. W. Clark and G. A. Burley, *Chem. Commun.*, 2015, **51**, 13028–13031.
38 S. Xiong, Y. Wang, J. Zhu, J. Yu and Z. Hu, *Langmuir*, 2015, **31**, 5504–5512.
39 L. Wu, W. Wu, X. Jing, J. Huang, D. Sun, T. Odoom-Wubah, H. Liu, H. Wang and Q. Li, *Ind. Eng. Chem. Res.*, 2013, **52**, 5085–5094.

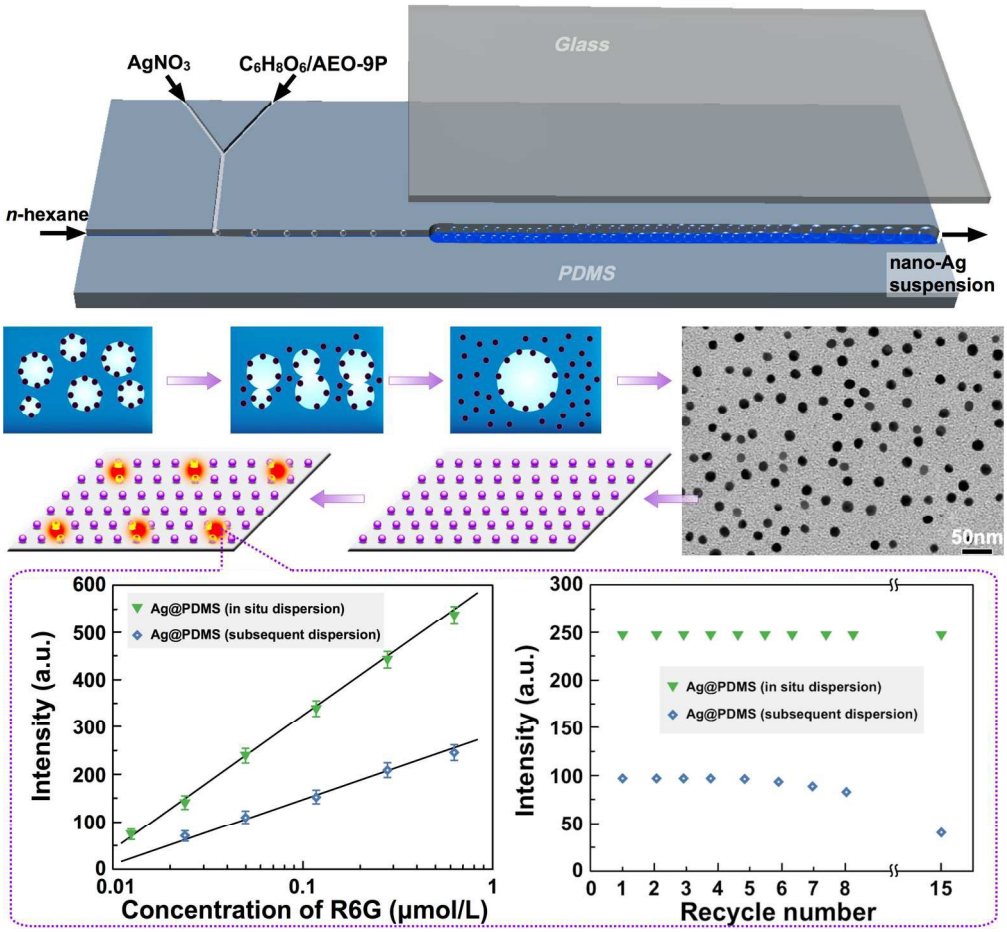

193x178mm (300 x 300 DPI)